

Chapter 1

Electrochemical Fabrication of Spherical AuNP-Tipped AFM Probes

As discussed in the previous chapter, nanostructuring a tip can create the necessary geometry and electromagnetic interfaces to support antenna-like plasmons. This enables coupling with far-field light and can improve the plasmonic performance of such tips. Consequently, this also means that excited plasmons scatter into the far-field and are therefore experimentally observable. This is a crucial property when using tips to measure fundamental plasmonics. Because of this, one of the major aims of this project is to produce robust nanostructured, plasmonic tips. The spherical geometry is targeted for its simplicity.

Fabrication of spherical tips has previously been achieved by mounting single nanoparticles onto the apices of tips. This concept has been reported numerous times over the last decade [1], beginning with the use of fibres as mounting structures [2–5] and progressing onto the use of scanning probe microscopy (SPM) tips [6–10]. Whilst mounting nanoparticles onto SPM tips is more difficult than with fibres the additional capabilities of the SPM tip have made such tips desirable. However, these tips typically require complicated assembly processes to precisely secure a single nanoparticle (NP) at the apex of the tip, greatly increasing their fabrication time and costs. More recent methods have attempted to address the complexity issue by directly depositing nanoparticles onto the apex by exploiting localised chemical reactions. Nevertheless, these techniques have still been limited by cost or required specialist equipment [4, 9], incompatible with SPM probes [3, 11] or subject to limitations in nanoparticle growth, either in size [12] or material [6]. Non-metallic spherical tips on atomic force microscopy (AFM) probes have been created using methods such as vacuum-processing diamond-like carbon growth (NanoTools B-series). These nanotips can then be made plasmonic through evaporation of a metallic coating. Even in recent years it still remains a challenge to simply and efficiently produce spherically nanostructured tips.

Electrochemical deposition is highly suited to the tip geometry because of the large field enhancement localised at the sharp apex point. Due to its significantly reduced radius of

curvature, the equipotential surface resulting from an applied voltage leads to the compression of field lines at the tip apex. This strongly increases the field amplitude in the vicinity of the tip apex and is known as the lightning rod effect. Under such conditions the rate of electrochemical reactions is significantly increased around the tip apex. By exploiting this localised field enhancement it is possible to grow a spherical metallic nanoparticle (MNP) directly onto the tip apex. Whilst use of the lightning rod effect for electrochemical growth has been used to grow dense forests of MNPs [13, 14] it has yet to be applied to the fabrication of single MNPs at a tip's apex.

Selective growth of MNPs onto the apices tips is difficult using traditional methods of electrochemical deposition but can instead be achieved by using single-pulse, high-field electrochemical growth. This chapter describes the process of pulsed electrodeposition for apex-selective nucleation and growth of AuNP AFM tips. The process of electrochemistry is first described followed by discussion of the method by which spherical AuNP-tipped AFM probes are produced.

1.1 Electrochemical Deposition

Electrochemistry is defined as the study and application of chemical reactions occurring on the surface of an electrode that are either caused by or generate an electrical current. Electrochemical growth, or electrodeposition, is a method of which for depositing a solid material from solution. In general, this requires two electrically connected electrodes, submerged in an ionic solution (electrolyte), with a potential difference. Depending on the electrode potential, and how it compares with the energy required to activate a specific chemical reaction between ionic species, ions are either removed or created at the electrode-electrolyte interface through the addition or removal of electrons, respectively. Electrically connecting electrodes allows excess electrons donated at the anode to transfer and fill the electron deficit at the cathode. An electrochemical cell reaction is therefore split into two half-reactions - electron capture and electron generation. These reactions are known as *oxidation* and *reduction*, which combine to form an overall *redox* reaction. Oxidation occurs at the anode whilst reduction occurs at the cathode. The current flow between electrodes at a given potential is therefore a measurable representation of the underlying reaction rate with electrode potentials setting the range of possible redox reactions. Thus, electrochemistry is a powerful technique, containing an in-built method of directly monitoring the state of the chemical process.

Each oxidation and reduction reaction has an associated standard potential, E° , characterising the potential required to add or remove an electron from the chemical species. Chemical species with highly negative standard potentials can readily donate electrons and are known as reducing agents. Chemical species with highly positive standard potentials are more likely to be reduced and are therefore known as oxidising agents. In general, having $E^\circ < 0$ means

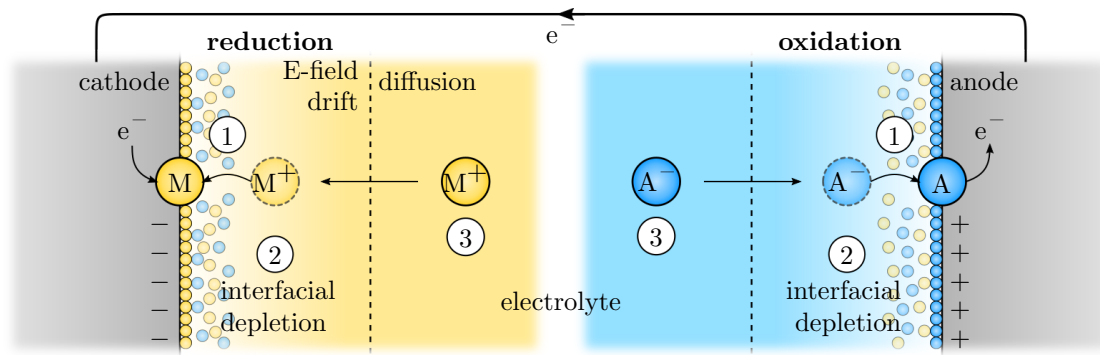


Figure 1.1: Diagram of the electrodeposition process over time. Two electrodes are submerged in an ionic solution. Depending on the potential, ions can either be oxidised or reduced at each electrode-electrolyte interface, generating a current between electrodes. Metallic ions initially at the interface are completely reduced on short time scales (1). Nearby ions drift to the surface following the field lines. Accumulation of the surface charge at the electrode leads to attraction of a diffuse layer of the oppositely charged ion, partially screening the local field. Depletion of ions in the vicinity of the surface (2) creates a concentration gradient. Further growth is limited by diffusion (3). The balance between drift-limited and diffusion-limited growth is determined by the concentration of the solution.

the chemical species is highly likely to dissociate into ions, while $E^\circ > 0$ means a chemical species is more likely to be found in a charge neutral or lesser charged state. Electrons move to equilibrate an in-built potential set by the difference between standard potentials at each electrode, $V_{\text{cell}} = E_{\text{ox}}^\circ - E_{\text{red}}^\circ$, and the resulting current can be used to power an external load.¹ This is the origin of the battery effect.

Electrodeposition is an opposite effect caused by either applying a voltage across a cell containing metal ions (standard electrodeposition) or by using a reducing agent (electroless deposition) [15]. If both redox half-potentials are overcome a redox reaction is activated. Metal ions from the solution are reduced onto the cathode surface, via a half-reaction,



in which n electrons are reacted with an n -oxidation state metal ion as a complimentary oxidation occurs at the anode. This is the basis of electroplating. Only electrode-based electrodeposition is discussed here in the context of electrodepositing onto tips.

A potential difference, $V_{\text{cell}} = E_{\text{ox}}^\circ - E_{\text{red}}^\circ$, needs to be applied to correctly bias the cell to overcome the activation energies of half-reactions at each electrode. Metallic ions situated at or near the cathode interface are then reduced whilst electrolyte ions on the anode surface oxidise.

¹Consider the example of a battery constructed of a Zn cathode and Cu anode in a Cu₂O/Zn₂O electrolyte connected via a salt bridge. The half-reactions are Cu²⁺ + 2e⁻ → Cu ($E^\circ = 0.339$ V) and Zn → Zn²⁺ + 2e⁻ ($E^\circ = -0.76$ V) with an overall reaction Zn + Cu²⁺ → Cu + Zn²⁺. The potential of this reaction is $\phi_{\text{Cu}} - \phi_{\text{Zn}} = 0.339 - -0.76 = 1.099$ V.

The rate of these reactions is set by a number factors, including the rate of charge transfer and nucleation. Excess surface charge accumulated at the electrode surface (unreacted metal ions from the solution and dissociated cathode ions) attracts a more diffuse layer of oppositely charged ions. This is known as the *electrical double layer* and partially screens the local potential, slowing down the rate of reaction [16]. After the initial surface reactions the rate of reaction becomes influenced by mass transport - the arrival of either ions or electrons at each interface. The arrival rate of electrons depends on any current limiting loads (circuit impedance) whilst the rate of ion movement is dictated by the electric field, ion concentration and electrophoretic mobility (**both forming the solution impedance**).² Nearby ions follow a trajectory to the electrode surface set by the field lines of the cell potentials. Local depletion of ionic species through reaction then leads to the formation of a concentration gradient towards the electrode. **Ions begin to diffuse along these gradients with an overall trajectory set by whether diffusive flow or electrical drift is stronger.** The extent of the ion depletion region is known as a diffusion zone and becomes important when two expanding diffusion zones overlap. Under these situations mass transport becomes divided between two competing growth sites, stunting growth.

In analogy with semiconductor physics the current density is given by the contributions of both diffusion and drift effects,

$$\mathbf{J} = q(n\mu_i \mathbf{E} + D\nabla n), \quad (1.2)$$

where q is the ion charge, n is the number density of charges (concentration), μ_i is the charge mobility and D is the coefficient of diffusion, therefore $v_{\text{drift}} = n\mu_i \mathbf{E}$ and $v_{\text{diffusion}} = D\nabla n$. Drift depends on the charge carrier concentration, the ion mobility and the electric field whereas diffusion depends only on the concentration gradient. Each component can therefore be controlled using the field strength and solution concentration. If the drift velocity is small compared to the diffusion velocity then the reaction is *diffusion-limited* and can be controlled by varying the concentration of the cell solution. Alternatively, if the diffusion velocity is small compared with the drift velocity, for example in the presence of a large field, then the reaction is field- or *drift-limited*. This becomes important when considering limitations on a reaction...

Electrodeposition is often described in terms of an *overpotential*, $\eta = E_{\text{applied}} - E^{\circ}$, that is the difference between the in-built potential of an electrolytic solution and the applied potential across it. In this case, E° is defined for the reduction of a metal ion onto an electrode of the same metal. Deposition of this metal will only occur once the applied potential is more negative than E° , i.e. $\eta < 0$. The more negative the overpotential the faster charge transfer, nucleation and drift will occur and therefore the faster the reaction will occur. However,

²Convection effects during mass transport are ignored for the purposes of this discussion.

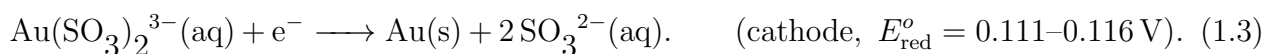
favourable interactions mean that some metals deposit easier onto electrodes made of other materials. In this case, deposition can begin even if $\eta > 0$. This is known as *underpotential* deposition and is useful to consider if a slow, controlled growth is desired.

1.1.1 Experimental Electrodeposition of Au

Electrodeposition is the process used to fabrication spherical Au AFM tips by exploiting the sharp profile of the tip apex. The dynamics of deposition depend heavily on the potential (electric field), the exposure time and the electrode/cell geometry and solution. In experimental electrochemistry, a potentiostat is used to apply or measure a controlled potential between two electrodes and the solution whilst also measuring the current through the cell. A reference electrode, with a well-known potential, is used to determine the individual potential of the working (active) electrode relative to the solution. The most fundamental reference electrode is the standard hydrogen electrode (SHE) since the dissociated of hydrogen is defined as $E^\circ = 0 \text{ V}$ [15], however, due to its complex setup, many other alternatives exist, including the saturated calomel electrode and the Ag/AgCl electrode. Potentials referenced using these other electrodes are often quoted relative to a SHE using the known reference potential. In the simplest of cells, reference electrodes can be in principle ignored and the counter electrode is used as a potential reference point.

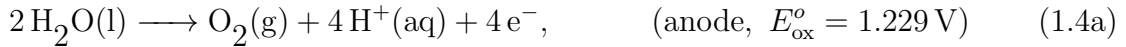
Au can be deposited using one of the many available precursor solutions. A simple precursor is AuCl_3 but it is not particularly widely used. A large number of solutions are cyanide based (e.g. AuCN), which pose significant health risks. Sulphite-based solutions ($\text{Au}(\text{SO}_3)_2^{3-}$) on the other hand are less hazardous at the cost of deposition quality. One of the most widely used sulphite-based Au precursors is the commercial ECF60 solution from Metalor. A smooth quality of the deposition morphology is typically achieved by slowly depositing in a low-potential (diffusion-limited) regime and using additives, such as brightener, to achieve smoother coatings [17]. However, when depositing nanostructures, additives are not necessary since the amount of Au deposited is typically very small. Additionally, ECF60 is water soluble [18], simplifying dilution for control over the Au ion concentration.

Since the actual composition of ECF60 is proprietary it's exact redox reaction is unknown. Known information includes it being a sulphite-based Au precursor consisting of 0.05 M Au and 0.24 M Na_2SO_3 at a pH of 9.5 [18]. The expected reduction reaction for a sulphite-based Au precursor is [19],

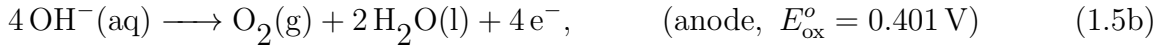


The redox reaction is expected to be satisfied by oxidation of the SO_3^{2-} species, however complementary water splitting reactions are also expected at higher potentials. Two sets of

half-reactions for the water splitting are [20],



and,



both resulting in a redox reaction of $2 \text{H}_2\text{O(l)} \longrightarrow 2 \text{H}_2(\text{g}) + \text{O}_2(\text{g})$. The standard potential of Eq. 1.4a is $E_{\text{ox}}^o = -1.23 \text{ V}$ ($E_{\text{red}}^o = 1.23 \text{ V}$ for Eq. 1.5a). In general, both these reactions occur simultaneously with a build up of H^+ at the anode and a build up of OH^- at the cathode. Using this solution, growth is expected to occur once $V < -0.6 \text{ V}$ [] with an increase in the number of reactions once $V < -1.23 \text{ V}$.

1.2 Initial Fabrication of Spherical AuNP-Tipped AFM Probes

Selective nucleation and growth of a single nanoparticle at the apex of an AFM tip requires using pulsed electrodeposition, an incredibly uncommon method. The reason for this is that standard methods are designed to produce an even metallic coating rather than growth at a single point. For tips, growth must initially be completely field dependent, taking advantage of the tip's lightning rod effect, but not over sufficient time that smoothing of the apex curvature takes place, reducing the apex field and diverting growth around the resultant neck. By applying a high potential in a short pulse all metallic surface ions are immediately reduced. Charge transfer in this domain can be considered instantaneous and nucleation readily takes place. Accumulation of surface charge therefore does not occur and thus the double layer never forms. Growth in this regime is only limited by mass transport.

A simple method is used to successfully demonstrate that a spherical AuNP can be electrochemically grown at the apex of a metallic AFM tip. Conductive coatings are required for the electrochemical reaction, therefore Au- and Pt-coated AFM tips are used (BudgetSensors GB/E series). The adhesion of molecular layers can prevent deposition of Au therefore tips must be cleaned thoroughly prior to deposition. Tips are pre-treated with 20 min O_2 plasma to remove organic contaminants from the surface prior to growth. A simplified two-electrode system (AutoLab PGSTAT 302N potentiostat) is employed for growth since both cell geometry and electrodeposition solution are kept the same between fabrications. AFM probes are

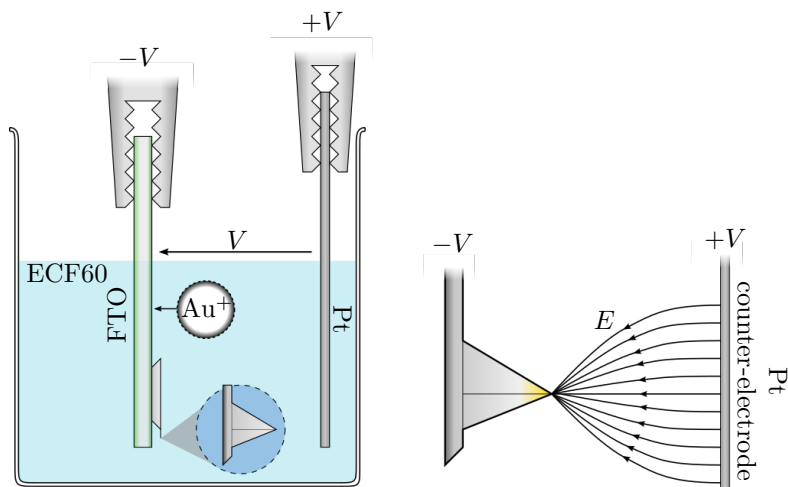


Figure 1.2: Experiment geometry for pulsed electrochemical deposition of Au onto an AFM tip. Electrochemical cell for growth of Au onto the apex of an AFM tip. Termination of field lines at tip apex due to the lightning rod effect enhances localised electrochemical growth for single NP growth.

attached to fluorine-doped tin oxide (FTO) conductive glass, used as a working electrode, opposite a Pt wire counter-electrode, spaced 10 mm apart (Figure 1.2). FTO glass is cleaned through sonication in 10 min steps using de-ionised (DI) water, ethanol and finally acetone. Metalor ECF60 is used as the electroplating solution with no additives. Simultaneous fabrication of both Au and Pt tips can be carried out by contacting multiple tips, closely spaced side-by-side on the same FTO surface.

Linear sweep voltammetry of a single AFM tip in ECF60 (Figure 1.3) shows that Au growth starts at around -1 V . This is larger than what is theoretically expected. Differences are attributed to the potentials being referenced to the counter electrode instead of the

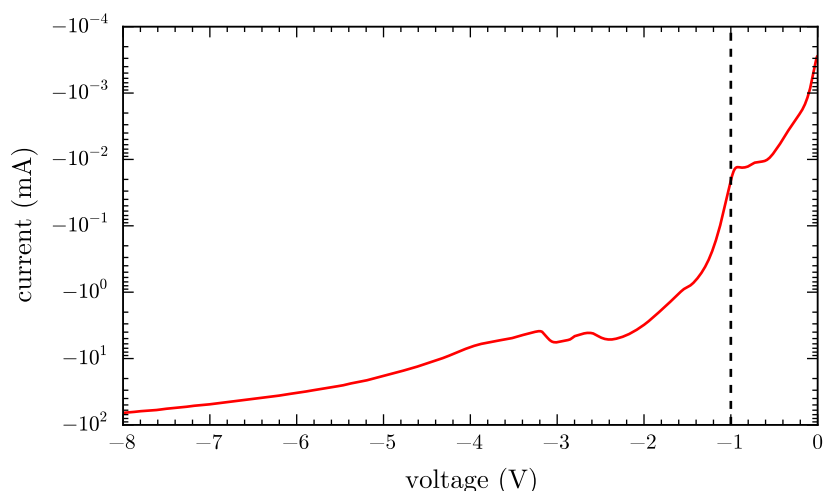


Figure 1.3: Linear sweep voltammetry of a single AFM cantilever in ECF60. The AFM probe is held by an Al clamp cathode out of solution, replacing the standard FTO electrode to show growth characteristics of only the tip. The remaining geometry is the same as in Figure 1.2.

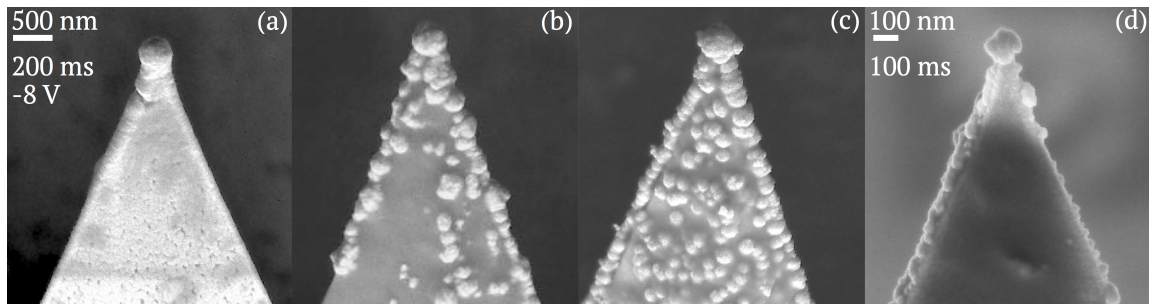


Figure 1.4: Comparison of AuNP-tipped AFM probes, fabricated on various base structures using -8 V pulses of different lengths. The first three tips were produced simultaneously using a 200 ms pulse on (a) a commercial Pt tip with no pre-treatment, (b) a plasma-treated Pt tip, (c) a plasma-treated Au tip. (d) Duplicate spherical tip produced separately on a plasma treated Pt tip using a 100 ms pulse.

solution, thus increasing the required potential difference. Further increases in growth are attributed to the activation of water splitting reactions, confirmed by the generation of bubbles at each electrode at higher potentials. An increase from theoretical reduction potentials can also be caused by temperature which factors into the reaction thermodynamics [15]. The current inevitably becomes limited by mass transport causing the observed saturation at highly negative potentials.

A single high-voltage pulse is applied to nucleate and grow a single AuNP at the tip apex. Due to the large field amplitude at the tip apex, field lines from across the cell terminate at the apex, inducing ions to drift towards the tip apex prior to undergoing reduction (Figure 1.2b). Multiple combinations of applied voltage and pulse times are investigated to optimise growth parameters. Growth of Au onto the AFM tip is confirmed by current dynamics, revealing a 2–3 ms initiation followed by relaxation to continuous diffusion-limited growth within a few 10s of milliseconds. Scanning electron microscopy (SEM) imaging, carried out on a LEO GEMINI 1530VP FEG-SEM Scanning Electron Microscope, is used to characterise the resulting growth morphology.

SEM images of four tip samples fabricated at -8 V are shown in Figure 1.4, three of which were fabricated simultaneously on one FTO glass slide, to show the effects of tip pre-treatment and exposure time in the applied field. These images demonstrate that spherical AuNP tips can be reliably fabricated using the proposed electrodeposition procedure. AuNP growth diameters between 150–450 nm are achieved using 100–200 ms pulses across the electrochemical cell on both Pt and Au tips. Evidence of growth localisation to the high field regions is clearly exhibited by the formation of spherical AuNPs at the tip apex. The morphologies obtained differ with and without plasma pre-treatment. Using tips as supplied leads to a smooth sphere at the tip apex, resulting from the lightning rod effect, followed by a broad neck and semi-uniform Au coating across the exposed surfaces of the tip (Figure 1.4a). Plasma treatment removes organic contamination and can also oxidise the surface [21, 22]. Removal

of contaminants prevents growth at defect sites. The formation of an insulating metal oxide layer prevents growth on surfaces, limiting growth only to sharp regions with a small radius of curvature (Figure 1.4b–d). These regions remain conductive and the electric field is large and highly localised. Because Au is more difficult to oxidise than Pt, the shielding effect is different for plasma-treated, Au-coated AFM probes, which exhibit significant localised nanoparticle growth on all exposed surfaces (Figure 1.4c). Longer pulse times result in bigger diameters of spherical AuNP, as shown in Figure 1.4b and Figure 1.4d. A 200 ms pulse leads to a spherical AuNP on the Pt tip with a diameter of \sim 450 nm (Figure 1.4b), while the diameter of the AuNP is 150 nm with a 100 ms pulse (Figure 1.4d).

1.2.1 Dependence of Tip Morphology on Voltage and Underlying Nucleation Mechanisms

To investigate the dependence of fabricated tip morphology on the pulsed voltage across the electrochemical cell, the growth of AuNP on Pt tips at different applied voltages is further studied. SEM images of such fabrications along with corresponding current transients are shown in Figure 1.5. Images show that apex-selected growth occurs only once the voltage is more negative than -3 V . This voltage dependence is attributed to changes in deposition mechanism with field strength. At low voltages ($V \geq -2\text{ V}$), electrodeposition forms smooth film coatings (Figure 1.5b) similar to direct-current electrodeposition. Under these conditions growth is dominant over nucleation and the field profile caused by the lightning rod effect is eventually evened out, yielding smooth rounded tips. Even with 500 ms exposure time no apex-selective growth is observed despite the charge transfer being equivalent to AuNP tip growths at more negative potentials.

The electrodeposition morphologies on tips fabricated at potentials more negative than -2 V can be understood to a certain degree by considering it as the boundary for nucleation. Additional insight can be provided by further considering the most common nucleation mechanisms known from AuNP growth on planar electrodes [23]. These are progressive and instantaneous nucleation. During progressive nucleation, nuclei form at a time t then grow, increasing the size of the diffusion zone around them, thereby preventing further nucleation within that zone. At the end of progressive nucleation there are many nuclei of different sizes due to the different times at which they each originally nucleated. During instantaneous nucleation all nuclei are formed at $t = t_0$ and then grow at the same rate until their diffusion zones overlap. The overlap of diffusion zones stunts growth as the finite ion flow is split between the two nuclei. For a sparse distribution of nuclei the end result is a set of equally sized particles. For more standard electrodeposition the current transients for progressive and instantaneous

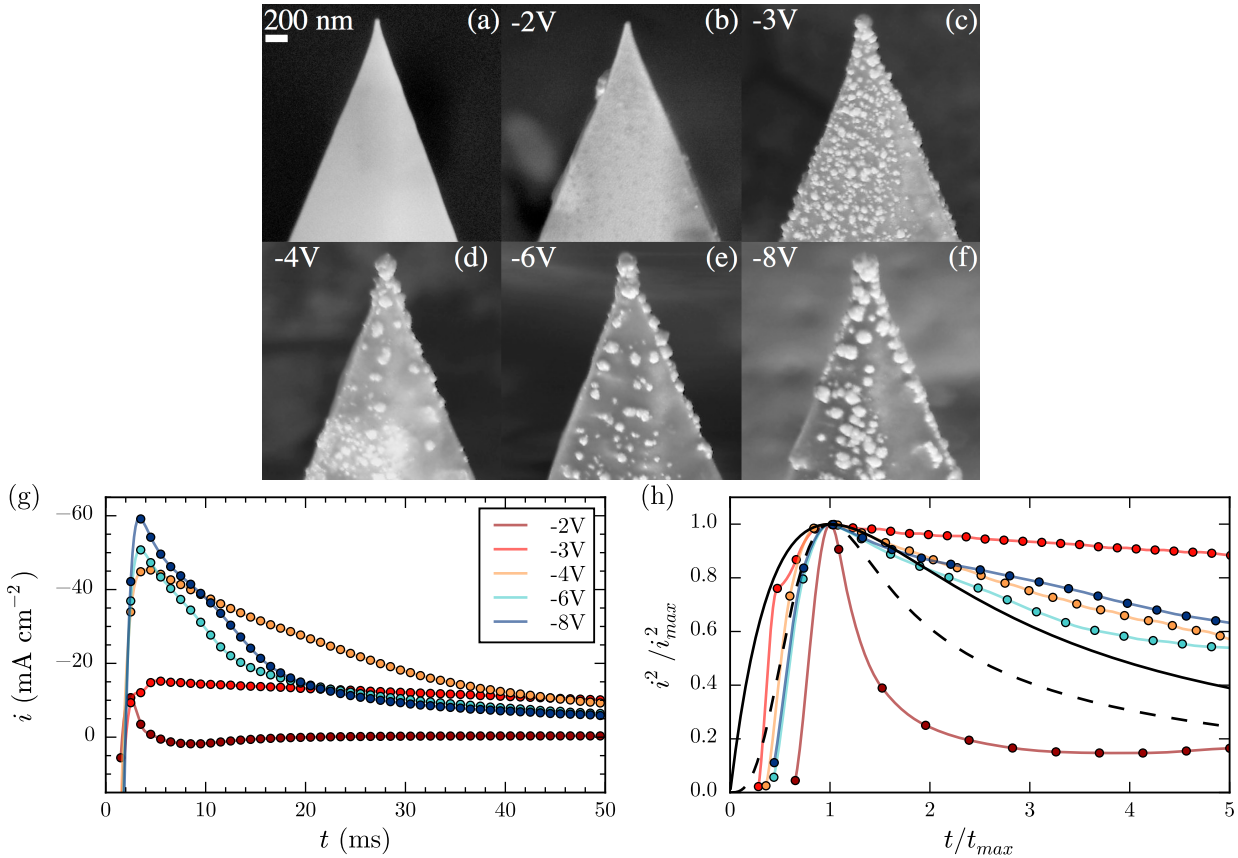


Figure 1.5: Voltage dependence of pulsed electrodeposition onto Pt tips. Comparison between a standard Pt AFM tip (a) and AuNP growth on plasma-treated Pt tips (b-f) using 150 ms pulses for voltages between -8 and -3 V and a 500 ms pulse at -2 V. This shows the change in deposition mechanism as the magnitude of applied field strength is increased, with no spherical growths above -3 V irrespective of exposure time. (g) Current transients from current traces measured during fabrication of tips shown in (b-f), offset by the saturation current density (-10 , -31 , -34 , -78 , -142 mA cm⁻², respectively). (h) Variable-independent reduced current transients (coloured lines) measured at various applied voltages during fabrication compared with theoretical curves for progressive (dashed) and instantaneous (solid) nucleation current transients [23].

nucleation are given in the Scharifker and Hills (SH) model by,

$$\left(\frac{i}{i_{max}}\right)^2 = \frac{1.2254}{t/t_{max}} \left[1 - e^{-2.3367(t/t_{max})^2}\right]^2, \quad (1.6)$$

and,

$$\left(\frac{i}{i_{max}}\right)^2 = \frac{1.9542}{t/t_{max}} \left[1 - e^{-1.2564(t/t_{max})}\right]^2, \quad (1.7)$$

respectively, where t_{max} is the time at which the current density maximises at i_{max} . Usually the boundary between these two cases is between -0.8 and -0.9 V [], however this behaviour has not been investigated on short time scales and large, negative potentials where conditions are severely different and the assumptions used to develop the SH model break down.

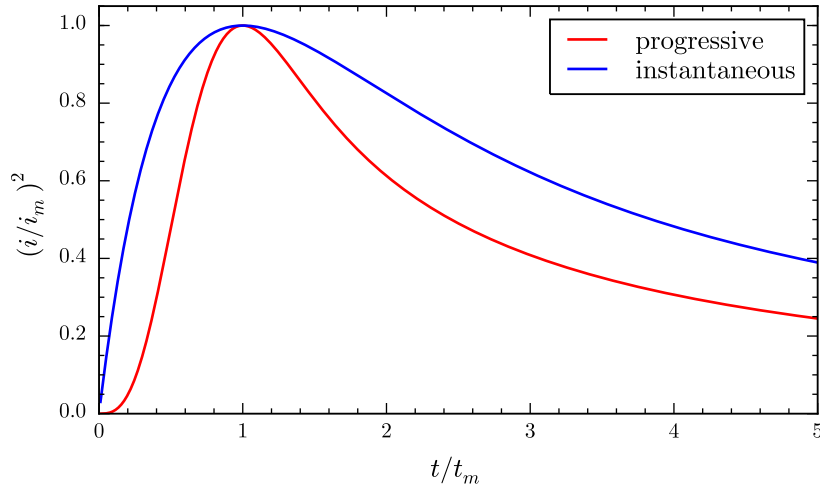


Figure 1.6: Reduced current transients for the two extremes of nucleation [23]. The normalised current, $(i/i_m)^2$, is plotted as a function of time normalised to the maximum, t/t_m . Dashed lines show reduced transients from linear transitions between instantaneous nucleation, assuming instantaneous nucleation occurs first then decreases.

Increased nucleation is observed at -3 V where spherical tip growth is initiated under a progressive nucleation mechanism. Some preferential growth is exhibited at the tip apex but a strong diffusion boundary has not yet formed, as evidenced by the large number of nucleated particles and variation in particle size (Figure 1.5c). For more negative voltages ($V \leq -4\text{ V}$) nucleation becomes more selective, leading to cleaner surfaces and improved apex localisation (Figure 1.5d-f). This is due to a transition to instantaneous nucleation, in which a fixed number of particles nucleate at selected active sites upon application of a field [24]. This occurs preferentially at sharp edges where the field is highest. Further selectivity may occur through depletion of ions in the vicinity of the growing tip, preventing additional growth sites. This helps to produce an isolated AuNP at the tip apex. Increasing the magnitude of the voltage increases the number of active sites available for nucleation and more of the tip surface surpasses the field threshold for instantaneous nucleation. Hence, using less negative voltages while still remaining in an instantaneous nucleation regime minimises the number of active nucleation sites, leading to cleaner spherical growth at the tip apex.

A changeover in nucleation mechanisms is also observed in current transients (Figure 1.5g)³ as the shape distinctly changes when decreasing the voltage below -2 V . The largest change in transient shape occurs at -3 V , indicating the onset of shorter time-scale nucleation. Elongation of the transient time is likely caused by contribution to the current from progressive particle nucleation throughout the exposure. Much sharper, short time-scale current transients are observed for potentials more negative than -4 V , supporting the hypothesis of an

³Current measurements are interpolated to create a smooth line through data points. Transients are analysed by first making a quadratic interpolation of experimental data points before data reduction to extract the reduced current transients. This approach is used due to the limited number of points available in the peak region.

instantaneous nucleation mechanism as the fast current decay indicates the saturation of all active sites, leaving only diffusion-limited growth.

The influence of instantaneous nucleation for isolated AuNP tip growth is further evident in comparisons to theoretical (SH model) reduced current transients for diffusion-limited progressive and instantaneous nucleation (Figure 1.5h). Reduced current transients are normalised to $(i/i_{\max})^2$ and plotted against t/t_{\max} to remove variable dependencies, where i_{\max} and t_{\max} represent the peak current and corresponding time. In general, for less negative deposition potentials (-2 V), nucleation resembles more closely progressive nucleation and growth, while at more negative potentials ($V < -4\text{ V}$) it resembles more closely instantaneous nucleation. This correlates well with the SEM images shown in Figure 1.5d-f. Variations from theory occur due to the variable field profile present across the tip leading to localised instances of both progressive and instantaneous nucleation contributing to the overall current. It should be known that the SH model is built upon assumptions such as random nucleation and provides valid results only for the limiting cases of only progressive or instantaneous nucleation, for which the validity fails in such a selectively grown system [25].

A simple model can be developed from SEM images and current transients. Whilst the large surface area of the FTO glass likely dominates the behaviour of the current density, SEM images do indeed show localised changes in the morphology of the tip. When the apex of the tip has a field profile above the threshold for instantaneous nucleation, a single particle may nucleate at the apex and quickly grow. As it nucleates quicker than the rest of the tip its diffusion zone increases to prevent other particles nucleating nearby. This leads to a clean single AuNP growth at the tip apex. If the threshold for instantaneous nucleation is not met then many smaller particles form around the apex (Figure 1.5c). On the other hand if too much of the tip nucleates instantaneously (very large overpotentials) then the chance for a clean growth is also heavily reduced (Figure 1.5f) since many particles nucleate around the apex prior to the expansion of substantial diffusion zones. The choice of voltage is therefore imperative to ensuring selective growth of a single AuNP at the apex.

1.2.2 Decontamination of Tip Surfaces and Post-Fabrication Processing

After each batch of fabrications, tips are imaged using SEM to study surface morphology. Characterisation is necessary to determine the specific apex morphology but leads to contamination issues. Exposure to the electron beam is known to deposit layers of carbon onto samples. Despite washing tips in DI water and ethanol after deposition to remove any leftover chemical films, the surface of the tip inevitably contains carbon contamination after imaging. To ensure good electrical contact, AuNP tips must be cleaned before use. Although plasma cleaning is used to remove organics from the surface before fabrication it can oxidise

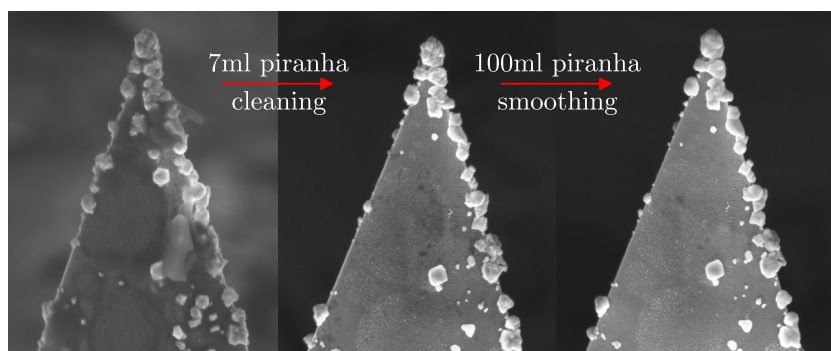


Figure 1.7: Post-processing effects of piranha solution. Low volume and temperature piranha solution removes organics from the Au surface while large volumes at 120 °C smooth the surface.

the surface. Submerging tips in piranha solution ($3\text{ H}_2\text{SO}_4 : 1\text{ H}_2\text{O}_2$) for 10 min proves to be an effective method for removing organics from the surface of the Au without introducing any adverse surface layers.⁴ Though it can still oxidise (or hydroxylate) surfaces it is to a lesser extent compared to plasma treatment. Tips treated with piranha solution electrically contacted more often than tips left untreated after SEM imaging.

The activity of piranha solution degrades over time with some indication that small volumes of the solution loses effectiveness after only 15 min. During its initial stages, the piranha reaction is extremely exothermic with temperatures reaching up to 120 °C. The overall temperature of the solution is determined by the volume of solution used. The heat generated in larger volumes takes longer to dissipate, maintaining a higher average solution temperature. The morphology of tips can be somewhat adjusted by exposing tips to piranha solution with varying temperatures and exposure times. Tips cleaned in small (5 ml) volumes show no changes in morphology whereas those treated in a large (100 ml) volumes are found to have smoothed surfaces (Figure 1.7). This effect is attributed to the increased solution temperature enabling surface atom rearrangement into more energetically favourable configurations. No comparison is made with other high-temperature solutions, such as boiling water, since the cleaning of tips is also desired. Should a fabrication fail, or their morphology damaged, Pt tips can be returned to their original state by using Au etching solution (Sigma standard Au etchant) to remove any deposited Au. This effectively reduces the effective cost per successfully nanostructured tip.

⁴Piranha solution is a strong oxidising agent and works via H_2SO_4 quickly dehydrating organics. H_2SO_4 and H_2O_2 react to create oxygen radicals which oxidise the remaining carbon molecules into elemental carbon. The overall result is the decomposition of organic matter into carbon, CO_2 and water.

1.3 Conclusions

By using electrochemical deposition, the simple fabrication of spherical metallic tips has been successfully demonstrated. Tips can be fabricated within a short period of time and with high throughput using pulsed electrochemical deposition, exploiting the sharp tip geometry to nucleate and grow a single nanoparticle at the apex. Though simple and cheap compared with many other techniques, control of growth morphology quality still presents issues. The many free variables in the system are problematic for morphology control and are yet to be fully understood and optimised. As a result, there is currently little ability to predict the size and shape of growths. Nevertheless, the deposition process succeeded in its original purpose of providing spherical AuNP tips for plasmonic applications that can be electrically contacted to measure charge transfer through a plasmonic nanogap.

Several advantages emerge from apex-selective single nanoparticle electrochemical growth. The capability for simultaneous nanoparticle growth on many tips ensures a high throughput process, while morphology and size is controlled by voltage and time. This provides a viable method for producing tips capable of expanding the user-base of plasmonics and furthering research into applications of TERS and SNOM. Furthermore, the spherical nanoparticle growth method introduced here is not restricted to specific metals, and many different composite systems can be created with this apex-localised growth technique. For example, silver nanoparticle tips could give a large optical response and field enhancement under visible illumination (although oxidation is sometimes an issue). This technique could therefore become a simple route to effectively improve TENOM across a broadband wavelength range.

References

- [1] Y. Gan, Review of scientific instruments **78**, 081101 (2007).
- [2] T. Kalkbrenner et al., Journal of Microscopy **202**, 72–76 (2001).
- [3] I. Barsegova et al., Applied Physics Letters **81**, 3461–3463 (2002).
- [4] O Sqalli et al., Journal of applied physics **92**, 1078–1083 (2002).
- [5] Y. Kawata et al., Applied physics letters **82**, 1598–1600 (2003).
- [6] T. Umakoshi et al., Applied Physics Express **5**, 052001 (2012).
- [7] N. Hayazawa, T.-a. Yano, and S. Kawata, Journal of Raman Spectroscopy **43**, 1177–1182 (2012).
- [8] C.-G. Park et al., B. Korean Chem. Soc **33**, 1748–1752 (2012).
- [9] T Okamoto and I Yamaguchi, Journal of microscopy **202**, 100–103 (2001).
- [10] I. U. Vakarelski and K. Higashitani, Langmuir **22**, 2931–2934 (2006).
- [11] S. Kharintsev et al., Journal of Physics D: Applied Physics **46**, 145501 (2013).
- [12] H.-W. Cheng et al., Nanoscale research letters **8**, 1–10 (2013).
- [13] Y. Tian et al., The Journal of Physical Chemistry B **110**, 23478–23481 (2006).
- [14] Y.-C. Yang et al., The Journal of Physical Chemistry C **115**, 1932–1939 (2011).
- [15] M. Paunovic and M. Schlesinger, *Fundamentals of electrochemical deposition*, 2nd ed., Vol. 45 (John Wiley & Sons, 2006).
- [16] A. J. Bard and L. R. Faulkner, *Electrochemical methods: fundamentals and applications*, 2nd (Wiley New York, 2001).
- [17] L Oniciu and L Mureşan, Journal of Applied Electrochemistry **21**, 565–574 (1991).
- [18] S Roy, ECS Transactions **16**, 67–72 (2009).
- [19] T. A. Green, Gold Bulletin **40**, 105–114 (2007).
- [20] “Crc handbook of chemistry and physics”, in, edited by W. M. Haynes (CRC press, 2013).
- [21] Z. Li et al., Surface science **529**, 410–418 (2003).
- [22] P Fuchs, Applied Surface Science **256**, 1382–1390 (2009).
- [23] B. Scharifker and G. Hills, Electrochimica Acta **28**, 879–889 (1983).
- [24] M. E. Hyde and R. G. Compton, Journal of Electroanalytical Chemistry **549**, 1–12 (2003).

- [25] P. V. Dudin, P. R. Unwin, and J. V. Macpherson, *The Journal of Physical Chemistry C* **114**, 13241–13248 (2010).